Modes and damping in cMUT transducers for acoustic emission

D.W. Greve and W. Wu
Department of Electrical and Computer Engineering
Carnegie Mellon University, Pittsburgh, PA, USA

I.J. Oppenheim
Department of Civil and Environmental Engineering,
Carnegie Mellon University, Pittsburgh, PA, USA

***Abstract*—Acoustic emissions caused by the initiation and growth of cracks can be detected by cMUT transducers. A particular advantage of this type of transducer is the possibility of fabricating transducers with multiple resonant frequencies. However previously reported designs had several modes within the frequency range of interest. In this paper we consider the design of an improved transducer which exhibits large spacing between resonant modes. In addition we discuss the prediction and measurement of the quality factor.**

Keywords-acoustic emission, transducer, MEMS, cMUT

I. INTRODUCTION

Acoustic emissions are ultrasonic pulses produced in solids when irreversible damage occurs under mechanical loading. Most commonly piezoelectric transducers with controlled damping are used to detect acoustic emissions [1] although alternative sensors have been explored [2,3,4,5]. We have previously reported the application of cMUT transducer arrays for the detection of acoustic emission events [6]. The cMUT array makes it possible to have multiple transducers that sample different portions of the broadband acoustic emission signal. Using the poly-MUMPS process, we designed and fabricated a cMUT transducer array consisting of polysilicon plates suspended by springs located inside the plate [6,7]. This design exhibited two electrically active modes within the frequency range of interest, and quality factors that were lower than desired. Here, we combine finite element simulation and experimental studies to understand the nature of the modes exhibited by these transducers, to quantify damping, and to compare the measured damping with an improved analytic model. These results lead to an improved transducer design for which we report the results of initial device characterization.

II. OLD DESIGN SIMULATIONS

We first consider the performance of a previous, non-optimized design (referred to as design #1 below). That design used the POLY0 and POLY1 layers of the poly-MUMPs process to form fixed and suspended electrodes, respectively. The operating principle of this transducer is similar to the cMUT in that a DC bias is applied and vibrations of the electrodes with respect to each other cause an electric current in the external circuit. However in contrast to the cMUT acoustic energy is coupled to the substrate and the upper electrode is free to move with respect to the lower electrode.

In order to obtain reasonable signal levels many small units are joined together to form a single large diaphragm. Figure 1 shows one unit, its connections to neighboring units, and a cross-section of the structure. Each unit consists of a POLY1 plate suspended from four supports. Transducers with different resonant frequencies are designed by varying the length of the springs and the total size of each unit. Figure 1 also shows etch release holes that are provided to enable removal of the sacrificial layer but which also have the effect of damping the diaphragm resonance.

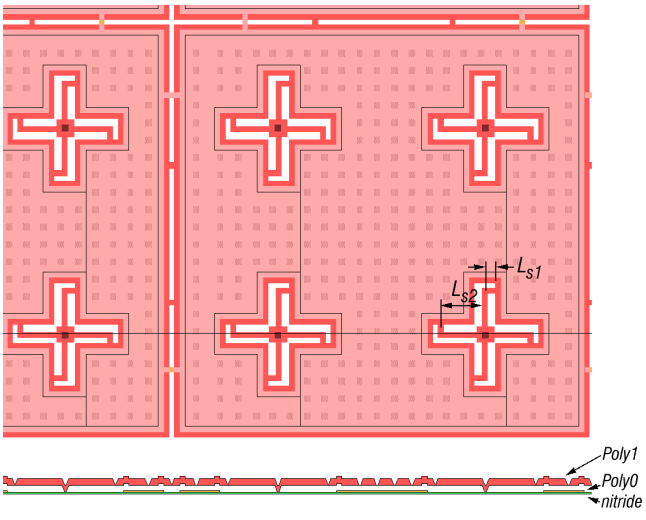

Figure 1. One unit of the diaphragm and connections to neighboring units.

Experiments with design #1 showed two important shortcomings. First, we observed that there were at least two closely spaced vibrational modes. And secondly, the damping in air was high resulting in low Q. Low Q leads to a wide bandwidth and in addition low sensitivity [6,7]. The purpose of this work is to understand the deficiencies of this design and to develop an improved transducer design.

In order to understand the vibrational modes, the eigenmodes were calculated using the structural mechanics module of FEMLAB. Figure 2 shows the results of simulations of one of the six transducers (unit size 310 × 310 μm, spring dimensions L_{s1} = 8 μm, L_{s2} = 27 μm). One quarter of a

unit is shown and the calculation assumed symmetry about the two rearmost edges.

The lowest predicted eigenmode (Fig. 1, top) is at 225 kHz which is in fair agreement with the measured lower resonant frequency of 187 kHz. Note that there is significant bending of the plate, that is, the motion is not simply the vibration of a rigid plate supported on springs. The second eigenmode at 261 kHz corresponds to a tilting motion of the entire unit and consequently this mode is electrically inactive. The next mode at 316 kHz is shown in the lower figure. Again the high degree of plate flexibility is evident. These simulations are consistent with our experimental observation of two closely spaced resonances [6,7]. These modes are closely spaced because the vibrational modes of the plate mass- spring system are close to the vibrational modes of a freely suspended plate. Consequently we have looked for other designs which have plates which are more rigid and/ or springs that are more flexible.

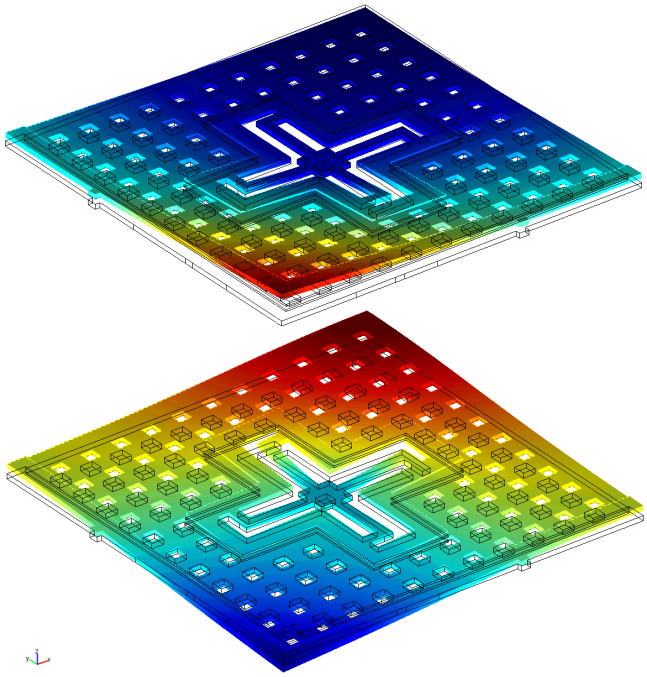

Figure 2. Design #1 fundamental mode (top) and third mode (bottom). Each figure shows the z displacement of the simulated eigenmode (color) and the undistorted structure (outline).

III. IMPROVED TRANSDUCER DESIGNS

Objectives for an improved design include (1) wider separation of the two lowest electrically active resonances and (2) decreased damping. To this end we considered two designs. Design #2 used only the POLY1 layer but the springs were moved to the edge and the size of each unit was reduced. Design #3 used both POLY1 and POLY2 plates to form the diaphragm. Simulation results for these two designs along with simulation results for the previous design are presented in Table I.

TABLE I. SIMULATION RESULTS FOR VARIOUS DESIGNS

	design 1 (expt)	design 1 (simulated)	design 2 POLY1 (simulated)	design 3 POLY1+POLY2 (simulated)
f_1 [kHz]	187	225	179	179
f_2 [kHz]	275	316	1024	1518

An improved separation of the lowest modes was obtained with both new designs. Figure 3 shows simulation results for design #2 which is the one chosen for fabrication. Again only one quarter of the structure is shown although in this case the symmetry planes were along the two edges at the right of the figure.

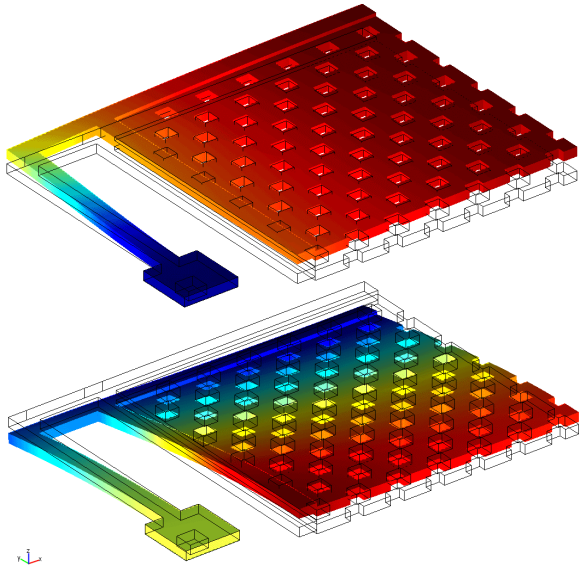

Figure 3. Design #2 fundamental mode (top) and next highest mode (bottom).

Transducers with a range of resonant frequencies have been designed with similar geometry using the single-poly diaphragm. Table II summarizes the dimensions and characteristics of these transducers.

TABLE II. TRANSDUCER DESIGN PARAMETERS AND COMPARISON OF PREDICTED AND MEASURED DYNAMIC PROPERTIES

spring length L_s [μm]	spring number n_s	f_{s1} [kHz] (simulated)	f_{s1} [kHz] (expt)	Q (predicted)	Q (expt)
56.5	4	126	116	3.3	2.4
28.5	4	255	232	6.6	3.6
17.5	4	351	311	8.9	3.4
10.0	4	404	345	9.8	5.4
10.5	8	500	443	12.6	4.9

IV. MODEL FOR Q PREDICTION

The quality factor Q of the diaphragm has a strong influence on the sensitivity, that is, the size of the output signal per unit velocity of the substrate [7]. We want the Q to have a moderate value as very high Q will lead to an excessively narrow bandwidth while low Q will result in poor sensitivity. For devices operated under atmospheric pressure, squeeze film damping associated with air flow into the gap region is a major contribution to the damping. In the following we outline a model for Q prediction.

We present an improved analytic model for the prediction of transducer Q which includes the effects of both edge and area damping. The model predictions will be compared with measurements of the damping at atmospheric pressure.

The quality factor Q is influenced by damping from several sources. We find

$$\frac{1}{Q} = \frac{1}{2\pi f \cdot m}(N \cdot c_{hole} + 2a \cdot c_{edge1} + 2a \cdot c_{edge2} + c_{rad}) \cdot$$

where f is the resonant frequency, m is the mass of a diaphragm unit, N is the number of etch release holes, and a is the edge length. In this expression

$$c_{hole} = -2\pi \int_{b_i}^{b_o} \{[\frac{r^2}{4} - \frac{b_i^2}{4} + (\ln b_i - \ln r)\frac{b_o^2}{2}]\frac{12\mu}{g^3}\} r dr$$

is the squeeze film damping associated with a single etch release hole [8], where b_i = 2.0 μm is the effective radius of the etch hole and b_o = 4.6 μm is the effective radius of the air volume flowing into each hole;

$$c_{edge1} = \frac{1}{3} \cdot \frac{12\mu}{g_e^3} b_{edge1}^3$$

and

$$c_{edge2} = \frac{1}{3} \cdot \frac{12\mu}{g_e^3} b_{edge2}^3$$

are the contributions to the damping per unit edge length; and

$$c_{rad} = Z_{air} A$$

is the contribution of acoustic radiation damping with A the diaphragm area. Here b_{edge1} = 8.0 μm and b_{edge2} = 4.5 μm are the effective distances for air flow at the diaphragm edges, μ = 18 × 10^{-6} Pa·s is the viscosity of the air at atmospheric pressure, Z_{air} = 430 kg/m^2·s is the acoustic impedance of the air, g = 1.25 μm is the gap beneath the diaphragm and g_e = 2.0 μm is the gap at the diaphragm edge. The various dimensions are defined in Fig. 4.

These expressions provide a basis for the design of acoustic emission transducers. For operation at atmospheric pressure, obtaining sufficiently high value for the Q is usually a major challenge. The Q increases with increasing N but with very large numbers of etch holes the diaphragm becomes more flexible and the capacitance per unit area decreases. So for a given diaphragm size, the challenge is to arrange the etch holes most effectively.

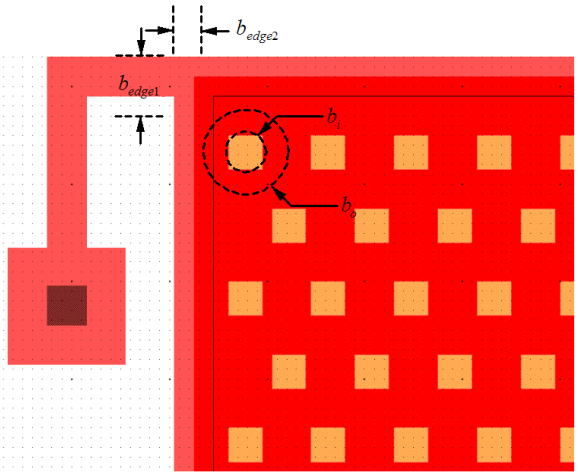

Figure 4. Detail of diaphragm edge showing effective distances for calculation of damping.

It is important to note that the radiation damping imposes a practical limit to the Q of a transducer operated at atmospheric pressure. We have chosen an etch hole size of 3.5 μm square arranged in a triangular array with approximately 8 μm hole spacing. The predicted values of Q for these dimensions are presented in Table II. Based on the Q model, a further increase in hole size or decrease in hole spacing does not greatly improve the Q value because the radiation damping begins to dominate.

V. EXPERIMENTAL RESULTS

We now discuss the preferred design developed based on the considerations above. We chose a single poly design because there was little advantage to be gained with a double-poly design. Transducers with five different resonant frequencies were designed with structure similar to that shown in Fig. 3. The plate size was kept constant at 125 × 125 micron square and the spring dimensions were varied in order to obtain different resonant frequencies. Each transducer consists of 144 diaphragm units that are coupled at the edges by small links to neighboring units. Based on the transducer area and the nominal gap the total capacitance is expected to be 13 pF. Table II summarizes the transducer resonant frequencies and dimensions.

The final chip design in the poly-MUMPS process is shown in Fig. 5. The 1 cm^2 die area was divided into four subdies with four transducers each.

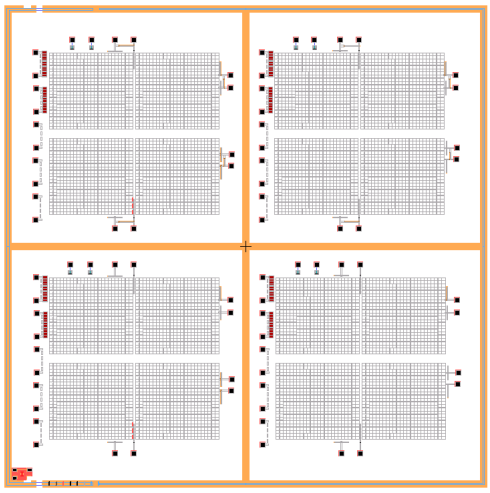

Figure 5. Chip design.

We now present the results of electrical characterization of the completed transducers. Released chips were bonded to a ceramic multigrid array package with an inverted chip cavity. This package is highly attractive for an acoustic emission transducer because it makes it possible to acoustically couple the flat surface of the package to the structure being studied. After bonding admittance measurements were made using an HP 4192A impedance analyzer. Measurements were performed with an applied DC bias of 12 V (351 kHz transducer) or 15 V (500 kHz transducer) under both atmospheric pressure and coarse vacuum.

Figure 6 presents typical results from two different transducers. The fundamental resonances are clearly observed both at atmospheric pressure and under coarse vacuum. As expected the resonances become considerably sharper under coarse vacuum. In contrast to our previous non-optimal design, only a single resonance is observed. Even under coarse vacuum conditions no higher resonance is observed at least up to 3 MHz (data at higher frequencies is not plotted in the figure for clarity).

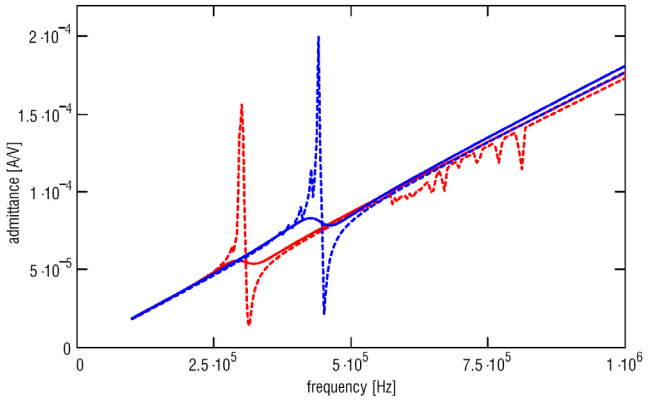

Figure 6. Measurements of the admittance magnitude as a function of frequency for two transducers: (—, – –) simulated resonance at 351 kHz and (—, – –) simulated resonance at 500 kHz.

Table II also presents the measurement results for the various transducers. The resonant frequencies and Q factors were determined by fitting the admittance measurements at atmospheric pressure to a single resonance. The measured resonant frequencies are in very good agreement with simulations. The Q values measured at atmospheric pressure are of the same magnitude but consistently somewhat lower than predicted. Even so, these results represent a significant improvement over the Q values obtained in our previous design.

Experimental characterization of the transducers in acoustic emission applications is presently in progress. The improved values of Q and single-mode resonance behavior are expected to contribute to improved sensitivity in this application.

VI. SUMMARY

We have developed an improved acoustic emission transducer design derived from the cMUT. The new design has a wide separation between the first and second electrically active modes. In addition, a model for the diaphragm damping has been developed and used to improve the quality factor. Experimental characterization of the fabricated transducers is consistent with simulations and theory. Application of these transducers to the detection of acoustic emissions is in progress.

ACKNOWLEDGMENT

We thank the Pennsylvania Infrastructure Technology Alliance and the National Science Foundation for support. This material is based upon work supported by the National Science Foundation under Grants No. CMS-0329880. Any opinions, findings, and conclusions or recommendations expressed in this material are those of the authors and do not necessarily reflect the views of the National Science Foundation.

REFERENCES

[1] G. Gautschi, *Piezoelectric Sensorics* (Berlin: Springer-Verlag, 2001).

[2] R.A. Kline, R.E. Green, and C.H.Palmer, "A Comparison of Optically and Piezoelectrically Sensed Acoustic Emission Signals," *J. Acoust. Soc. Amer.* **64** 1633-1639 (1978).

[3] Y.C. Yang and K.S. Han, "Damage Monitoring and Impact Detection using Optical Fiber Vibration Sensor," *Smart Materials and Structures* **11** 337-345 (2002).

[4] F.R. Breckenridge and M. Greenspan, "Surface-wave Displacement: Absolute Measurements using a Capacitive Transducer," *J. Acoust. Soc. Amer.* **69** 1177-1185 (1981).

[5] A.R. D. Jones, R.A. Noble R. J. Bozeat, and D.A. Hutchins, "Micromachined Ultrasonic Transducers for Damage Detection in CFRP Composites," *Proc. SPIE* **3673** 369-78 (1999).

[6] D. Ozevin, S.P. Pessiki, D.W. Greve, and I.J. Oppenheim, "Adapting a cMUT transducer to detect acoustic emissions," *2005 IEEE Ultrasonics Symposium* (Rotterdam, October, 2005).

[7] D. Ozevin, D.W. Greve, I.J. Oppenheim, and S.P. Pessiki, "Resonant capacitive MEMS acoustic emission transducers," (to be published in *Journal of Smart Materials and Structures*).

[8] I.J. Oppenheim, A. Jain, and D.W. Greve, "Electrical Characterization of Coupled and Uncoupled MEMS Ultrasonic Transducers," *IEEE Trans. Ultrasonics, Ferroelectrics, Frequency Control* **50** 297-304 (2003).

[9] **DO NOT REMOVE THIS PAGE**

---

[1] G. Gautschi, *Piezoelectric Sensorics* (Berlin: Springer-Verlag, 2001).
[2] R.A. Kline, R.E. Green, and C.H.Palmer, "A Comparison of Optically and Piezoelectrically Sensed Acoustic Emission Signals," *J. Acoust. Soc. Amer.* **64** 1633-1639 (1978).
[3] Y.C. Yang and K.S. Han, "Damage Monitoring and Impact Detection using Optical Fiber Vibration Sensor," *Smart Materials and Structures* **11** 337-345 (2002).
[4] F.R. Breckenridge and M. Greenspan, "Surface-wave Displacement: Absolute Measurements using a Capacitive Transducer," *J. Acoust. Soc. Amer.* **69** 1177-1185 (1981).
[5] A.R. D. Jones, R.A. Noble R. J. Bozeat, and D.A. Hutchins, "Micromachined Ultrasonic Transducers for Damage Detection in CFRP Composites," *Proc. SPIE* **3673** 369-78 (1999).
[6] our last UFFC AE
[7] D. Ozevin, D.W. Greve, I.J. Oppenheim, and S.P. Pessiki, "Resonant capacitive MEMS acoustic emission transducers," (to be published in *Journal of Smart Materials and Structures*).
[8] I.J. Oppenheim, A. Jain, and D.W. Greve, "Electrical Characterization of Coupled and Uncoupled MEMS Ultrasonic Transducers," *IEEE Trans. Ultrasonics, Ferroelectrics, Frequency Control* **50** 297-304 (2003).